July 1999

ELSEVIER

Materials Letters 40 (1999) 27–32

MATERIALS LETTERS

www.elsevier.com/locate/matlet

A study on the machinability of a $Ti_{49.6}Ni_{50.4}$ shape memory alloy

S.K. Wu [a,*], H.C. Lin [b], C.C. Chen [a]

[a] *Institute of Materials Science and Engineering, National Taiwan University, Taipei 106, Taiwan*
[b] *Department of Materials Science, Feng Chia University, Taichung 400, Taiwan*

Received 28 April 1998; received in revised form 22 January 1999; accepted 25 January 1999

Abstract

The machinability of a $Ti_{49.6}Ni_{50.4}$ shape memory alloy (SMA) has been studied by using a mechanical cutting test. There is a wide hardened layer in front of the cutting edge of the $Ti_{49.6}Ni_{50.4}$ SMA which comes from the effects of strain hardening and cyclic hardening. Meanwhile, $Ti_{49.6}Ni_{50.4}$ fragments can adhere on the diamond blade. The longer the cutting time, the more adhesion the $Ti_{49.6}Ni_{50.4}$ fragments have. These features cause the $Ti_{49.6}Ni_{50.4}$ SMA to exhibit more difficult cutting characteristics than 18-8 stainless steel and $Ti_{50}Al_{50}$ alloy. From the viewpoint of cutting energy, the effect of applied load is more important than that of cutting speed and there is an optimal cutting load for the cutting of $Ti_{49.6}Ni_{50.4}$ SMA.

Keywords: TiNi shape memory alloy; Cutting machinability; Hardening layer; Strain hardening; Cyclic hardening; Cutting load and speed

1. Introduction

TiNi alloys are an important class of shape memory alloys (SMAs). They exhibit not only shape memory effect (SME) [1], but also unusual pseudoelasticity [2,3] and high damping capacities [4,5]. These properties along with their superior ductility, fatigue strength, and corrosion resistance, have resulted in many applications. The basic characteristics of TiNi SMAs, involving transformational crystallography, shape memory phenomena, and the effects of thermo-mechanical treatments, have been intensively investigated [6–20]. However, the roadblocks to their development are caused by difficulties in the manufacturing process. It is well known that TiNi alloys can be tensile-deformed in a ductile manner to about 50% strain prior to fracture [1], but the severe strain hardening and the unique pseudoelastic behavior may cause the machining characteristics of TiNi SMAs to be quite complicated. To the best of our knowledge, no systematic investigation of the machining characteristic of TiNi SMAs has yet been reported, although some papers have reported their wire-drawing behavior [21–23]. In the present study, we aim to investigate the machinability of TiNi SMAs by using a mechanical cutting test and to discuss their optimal cutting parameters.

2. Experimental procedure

The conventional tungsten arc-melting technique was employed to prepare $Ti_{49.6}Ni_{50.4}$ SMA and $Ti_{50}Al_{50}$ intermetallics (in at.%). Titanium (99.7 wt.%), nickel (99.98 wt.%) and aluminum (99.99 wt.%), totaling nearly 100 g, were melted and

* Corresponding author. Fax: +886-2-363-4562

00167-577X/99/$ - see front matter
PII: S0167-577X(99)00044-0

remelted at least six times in an argon atmosphere. The mass loss during the melting was negligible. The as-melted buttons were homogenized at 1050°C × 24 h for the $Ti_{49.6}Ni_{50.4}$ alloy and at 1200°C × 50 h for the $Ti_{50}Al_{50}$ alloy, and then quenched in water. Rod specimens for mechanical cutting, 6-mm in diameter, were carefully prepared from these buttons. These specimens were vacuum-sealed in quartz tubes, annealed at 800°C for 2 h and then quenched in water.

The mechanical cutting was carried out by using an ISOMET 2000 Precision Saw made by BUEHLER, USA, and equipped with an automatic cooling and saw-grinding system. The rotation speed and applied load of the cutting saw (diamond blade No. 11-4276) are digitally controlled. The lubricant used during cutting was nine parts water to one part ISOCUT PLUS FLUID, BUEHLER. The microstructure observations of the cut specimens were made by an optical microscope (OM) and a scanning electron microscope (SEM). SEM observation was carried out with a JOEL-T100 microscope operated at 30 kV and equipped with an EDX analysis system. Specimens for hardness tests were mechanically polished and measured in a Vickers microhardness tester with a 500-g load. For each specimen, the average hardness value was obtained from at least five test readings.

3. Results and discussions

To understand the cutting characteristics of TiNi SMAs, some important mechanical properties of $Ti_{49.6}Ni_{50.4}$ alloy used in this study are presented in Table 1. Additionally, mechanical properties of 18-8 stainless steel (commercial available 304 grade) and $Ti_{50}Al_{50}$ intermetallics are also presented in Table 1 for comparison. Table 1 indicates that 18-8 stainless steel and $Ti_{49.6}Ni_{50.4}$ alloy exhibit good ductility, but $Ti_{50}Al_{50}$ alloy exhibits a brittle behavior. Although $Ti_{49.6}Ni_{50.4}$ SMA has the highest hardness (HV 255), the tensile strength of $Ti_{50}Al_{50}$ alloy is much higher than that of $Ti_{49.6}Ni_{50.4}$ alloy or 18-8 stainless steel.

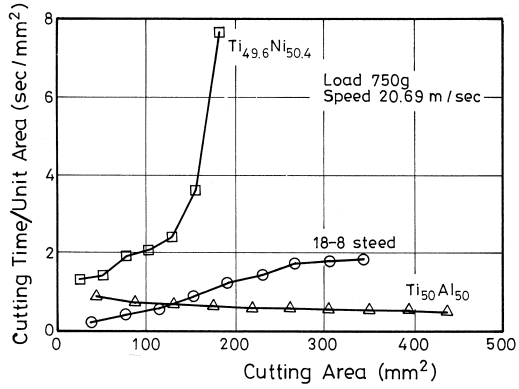

Fig. 1. The time needed to cut unit area (mm^2) of specimens at various cutting areas for $Ti_{49.6}Ni_{50.4}$ alloy, 18-8 stainless steel and $Ti_{50}Al_{50}$ intermetallics.

Fig. 1 shows the cutting time per unit area (s/mm^2) vs. the cutting areas for specimens of $Ti_{49.6}Ni_{50.4}$ alloy, 18-8 stainless steel and $Ti_{50}Al_{50}$ intermetallics. Here, the cutting area is the accumulated area cut by the same diamond blade. For each

Table 1
The important mechanical properties of $Ti_{49.6}Ni_{50.4}$ alloy, 18-8 stainless steel and $Ti_{50}Al_{50}$ intermetallics

Mechanical properties at room temperature	$Ti_{49.6}Ni_{50.4}$ SMA	18-8 Stainless steel	$Ti_{50}Al_{50}$ intermetallics
Structure (phase)	B2 phase	FCC Austenite	$L1_o$ γ phase
Hardness (HV)	255	190	230
Tensile strength (MPa)	190	120	450
Elongation (%)	22	27	1.5

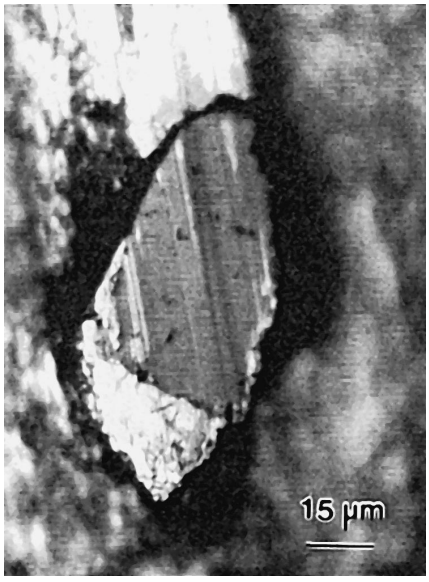

Fig. 2. An optical micrograph showing adhered fragments of $Ti_{49.6}Ni_{50.4}$ SMA or 18-8 steel on the surface of the diamond blade.

cut of the specimen it can accumulate about 28.3 mm^2 area due to the specimen being 6 mm in diameter. In Fig. 1, the cutting time per unit area of $Ti_{49.6}Ni_{50.4}$ specimen increases very quickly with increasing cutting area. The diamond blade even stops feeding after the cutting area reaches about 150 mm^2. For 18-8 stainless steel, the cutting time per unit area is found to slightly increase with increasing cutting area. Because of their high ductility, some

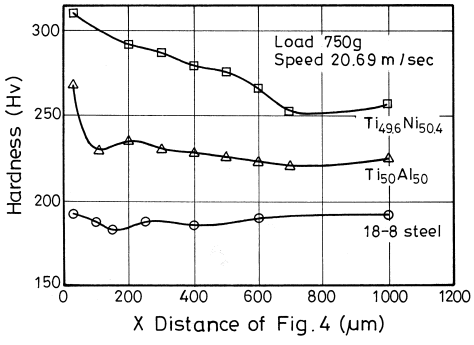

Fig. 3. Hardness at various distances X from the cutting edge of $Ti_{49.6}Ni_{50.4}$ SMA, 18-8 stainless steel and $Ti_{50}Al_{50}$ intermetallics.

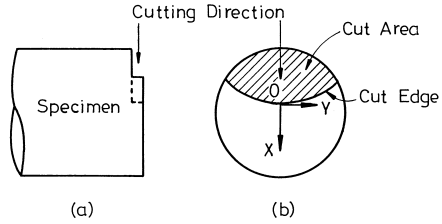

Fig. 4. Diagram showing the position for the hardness measurement: (a) side view, (b) cross-section.

cut fragments of $Ti_{49.6}Ni_{50.4}$ alloy and 18-8 stainless steel adhere to the diamond blade during cutting, as shown in Fig. 2. These adhered fragments will impede further cutting. The greater the cutting area, the more adhered fragments and hence the cutting time per unit area increases for these two materials. This feature is especially true for the $Ti_{49.6}Ni_{50.4}$ alloy. On the other hand, $Ti_{50}Al_{50}$ intermetallics exhibit a brittle behavior and $Ti_{50}Al_{50}$ fragments are not found to adhere to the diamond blade during cutting. In addition, the brittle fragments of $Ti_{50}Al_{50}$ alloy may have a grinding effect on the diamond blade. Hence, the cutting time per unit area of $Ti_{50}Al_{50}$ specimen even decreases with increasing cutting area, as shown in Fig. 1.

Fig. 3 shows the specimen's hardness vs. the distance X from the cut edge of $Ti_{49.6}Ni_{50.4}$ alloy, 18-8 stainless steel and $Ti_{50}Al_{50}$ intermetallics. The measured position X is illustrated in Fig. 4. In Fig. 3, the $Ti_{49.6}Ni_{50.4}$ alloy exhibits a severe hardening effect near the cutting edge. This characteristic is suggested to come from the effects of strain hardening and fatigue hardening during cutting, as discussed in Fig. 5. Fig. 5 plots the stress–strain curves

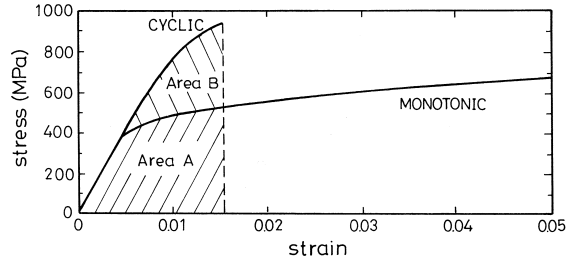

Fig. 5. Stress–strain curves showing the phenomena of strain hardening and fatigue hardening appearing in $Ti_{49.6}Ni_{50.4}$ alloy [24].

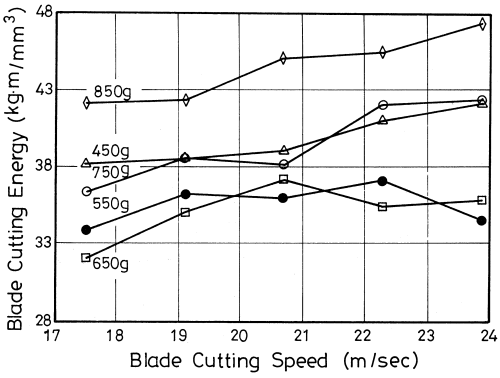

Fig. 6. The cutting energy vs. the blade cutting speed for various cutting loads.

of $Ti_{50}Ni_{50}$ alloy under the tensile (monotonic) test and cyclic (fatigue) test [24]. From Fig. 5, for strain ≤ 0.015, strain hardening occurs in the specimen of the monotonic test, as shown in region A. However, both strain hardening and fatigue hardening are induced in the specimen of the fatigue test, as shown by the regions A and B, respectively. We believe that the vibration induced by the cutting machine during the cutting process will cause a cyclic loading on the $Ti_{49.6}Ni_{50.4}$ alloy. Therefore, from Fig. 5, both strain hardening and fatigue hardening concurrently cause a severe hardening effect on the cutting edge. At this time, a wide hardening layer forms and its thickness can reach 700 μm in the $Ti_{49.6}Ni_{50.4}$ alloy, as shown in Fig. 3. The formation of this wide hardening layer during cutting can reduce cutting efficiency. This is the another reason why the cutting time per unit area increases significantly with increasing cutting area in $Ti_{49.6}Ni_{50.4}$ alloy, as shown in Fig. 1. On the other hand, Fig. 3 shows the specimen hardness of 18-8 stainless steel near the cutting edge has obviously not changed during cutting. We suggest that 18-8 steel does not have as severe a hardening effect as $Ti_{49.6}Ni_{50.4}$ alloy. Hence, Fig. 1 shows that the 18-8 stainless steel has better cutting behavior, although some fragments of 18-8 stainless steel can adhere to the diamond blade. For the $Ti_{50}Al_{50}$ intermetallics, a thin hardened layer with a sharp drop of hardness is observed near the cutting edge, as shown in Fig. 3. This sharp variation of hardness causes the hardened layer to spall off easily from the matrix and thus enhances the cutting rate.

Fig. 6 shows the cutting energy for the $Ti_{49.6}Ni_{50.4}$ alloy under various cutting loads and cutting speeds. The cutting energy is defined as (cutting load) × (cutting speed)/(cutting volume). Here, the cutting volume is the product of the cut area and the thickness of the blade. The blade used in this study is 0.5 mm in thickness. As shown in Fig. 6, the cutting speed has little effect, but the cutting load has a significant impact on the cutting energy. In general, it takes less time to cut commercial alloys (such as carbon steels or aluminum alloys) by using a higher cutting load or a higher cutting speed and therefore the cutting energy decreases with increasing cutting load or speed for these commercial alloys [25]. By using a lower blade cutting load as in region A of

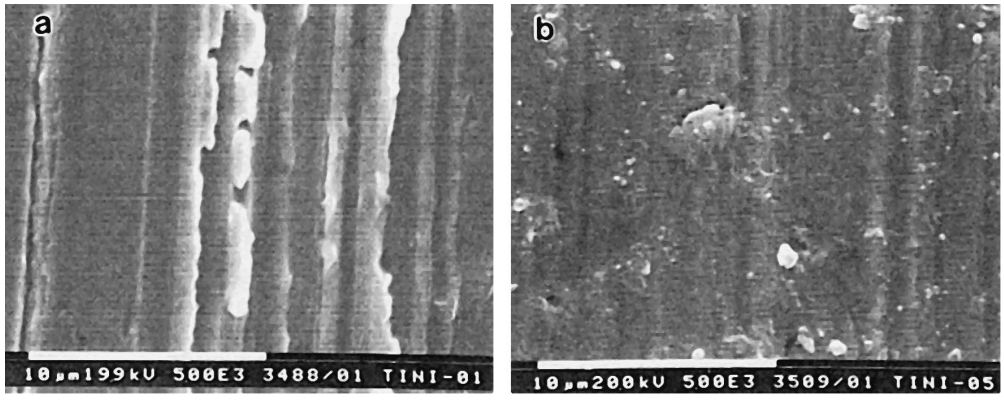

Fig. 7. Specimen's surface morphologies after the cutting of $Ti_{49.6}Ni_{50.4}$ alloy: (a) the ploughing grooves, and (b) the surface pits.

Fig. 5, the strain hardening is a dominant contribution to cutting. In this region, the cutting behavior of $Ti_{49.6}Ni_{50.4}$ alloy is similar to that of commercial alloys mentioned above, and hence the cutting energy decreases with increasing cutting load. However, if the cutting load is higher than a critical value, such as in region B of Fig. 5, both strain hardening and fatigue hardening will concurrently occur during cutting. At this time, severe hardening will impede the cutting process. Hence, the cutting behavior becomes worse and the cutting energy becomes higher in this case. This phenomenon indicates that there is an optimal cutting load in cutting $Ti_{49.6}Ni_{50.4}$ alloy. This optimal cutting load is found to be 550–650 g, as shown in Fig. 6.

Fig. 7a and b show the specimen's surface morphology after cutting $Ti_{49.6}Ni_{50.4}$ alloy. The ploughing grooves in Fig. 7a indicate the appearance of abrasive and ploughing wear in the cut $Ti_{49.6}Ni_{50.4}$ alloy. In Fig. 7b, many surface pits are observed. These surface pits originate from the adhesion of $Ti_{49.6}Ni_{50.4}$ fragments onto the diamond blade. The higher the cutting load, or the longer the cutting time, the greater the number of surface pits. This kind of adhesion impedes further cutting and helps to explain why the $Ti_{49.6}Ni_{50.4}$ alloy exhibits a more difficult cutting behavior.

4. Conclusions

The machinability of a $Ti_{49.6}Ni_{50.4}$ SMA has been studied by using a mechanical cutting test on an ISOMET 2000 Precision Saw. The machinability of 18-8 stainless steel and that of $Ti_{50}Al_{50}$ intermetallics are also compared. The important conclusions are as follows.

(1) There is a wide hardened layer in front of the cutting edge of the $Ti_{49.6}Ni_{50.4}$ alloy during cutting, which comes from the effects of strain hardening and cyclic hardening. Meanwhile, $Ti_{49.6}Ni_{50.4}$ fragments adhere to the diamond blade. The longer the cutting time, the more the adhesion of $Ti_{49.6}Ni_{50.4}$ fragments. These features cause the $Ti_{49.6}Ni_{50.4}$ SMA to exhibit difficult cutting characteristics. From the data concerning the cutting time per unit area vs. the cutting area, the $Ti_{49.6}Ni_{50.4}$ alloy is indeed found to be much more difficult to cut than 18-8 stainless steel and $Ti_{50}Al_{50}$ intermetallics.

(2) From the viewpoint of cutting energy for $Ti_{49.6}Ni_{50.4}$ SMA, the effect of the applied load on cutting is more important than that of the cutting speed. There is an optimal cutting load in this study and this load is found to be 550–650 g.

Acknowledgements

The authors are pleased to acknowledge the financial support of this research by National Science Council (NSC), Republic of China, under the Grant NSC85-2216-E002-023.

References

[1] S. Miyazaki, K. Otsuka, Y. Suzuki, Scr. Met. 15 (1981) 287–292.
[2] S. Miyazaki, Y. Ohmi, K. Otsuka, Y. Suzuki, ICOMAT-82, J. Phys. 43 (1982) C4-255-60.
[3] S. Miyazaki, T. Imai, Y. Igo, K. Otsuka, Met. Trans. 17 (1986) 115–120.
[4] H.C. Lin, S.K. Wu, Y.T. Yeh, Met. Trans. 24A (1993) 2189–2194.
[5] H.C. Lin, S.K. Wu, Y.C. Chang, Met. Trans. 26A (1993) 851–858.
[6] T. Tadaki, Y. Nakada, K. Shimizu, Trans. Jpn. Inst. Met. 28 (1987) 883–890.
[7] S. Miyazaki, Y. Igo, K. Otsuka, Acta Met. 34 (1986) 2045–2051.
[8] S.K. Wu, H.C. Lin, T.S. Chou, Acta Met. 38 (1990) 95–102.
[9] M. Nishida, T. Honma, Scr. Met. 18 (1984) 1293–1298.
[10] M. Nishida, C.M. Wayman, T. Honma, Scr. Met. 18 (1984) 1389–1394.
[11] S.K. Wu, H.C. Lin, Scr. Met. Mater. 25 (1991) 1295–1298.
[12] Y. Okamota, H. Hamanaka, F. Miura, H. Tamura, H. Horikawa, Scr. Met. 22 (1988) 517–520.
[13] T. Todoroki, H. Tamura, Trans. Jpn. Inst. Met. 28 (1987) 83–94.
[14] H.C. Lin, S.K. Wu, T.S. Chou, H.P. Kao, Acta Met. Mater. 39 (1991) 2069–2081.
[15] H.C. Lin, S.K. Wu, Acta Met. Mater. 42 (1994) 1623–1630.
[16] E.K. Eckelmeyer, Scr. Met. 10 (1976) 667–672.
[17] R. Wasilewski, in: J. Perkin (Ed.), Shape Memory Effects In Alloys, Plenum, New York, 1975, pp. 245–271.
[18] C.M. Hwang, M. Meichle, M.B. Salamon, C.M. Wayman, Philos. Mag. 47A (1983) 9–31.
[19] S.K. Wu, C.M. Wayman, Metallography 20 (1987) 359–376.

[20] K. Enami, T. Yoshida, S. Nenno, in: Proc. ICOMAT-86, The Japan Inst. Metals, Japan, 1987, pp. 103–108.
[21] Y. Kawaguchi, K. Katsube, M. Murahashi, Y. Yamada, Wire J. Int. 12 (1992) 53–58.
[22] S. Saito, T. Wachi, S. Hanada, Mater. Sci. Eng. A 161 (1993) 91–96.
[23] S.K. Wu, H.C. Lin, Y.C. Yen, Mater. Sci. Eng. A 215 (1996) 113–119.
[24] P. Clayton, Wear 202 (1993) 162–164.
[25] S.K. Wu, H.C. Lin, Y.C. Yen, unpublished work, 1996.